



Research Repository UCD

Title	Estimation of transitory changes in bending stiffness using the Hilbert-Huang transform
Authors(s)	González, Arturo, Aied, Hussein
Publication date	2019-12-31
Publication information	González, Arturo, and Hussein Aied. "Estimation of Transitory Changes in Bending Stiffness Using the Hilbert-Huang Transform." IOS Press, December 31, 2019. https://doi.org/10.3233/brs-190163 .
Publisher	IOS Press
Item record/more information	http://hdl.handle.net/10197/11509
Publisher's statement	The final publication is available at IOS Press through http://dx.doi.org/10.3233/brs-190163
Publisher's version (DOI)	10.3233/brs-190163

Downloaded 2025-12-04 23:03:37

The UCD community has made this article openly available. Please share how this access benefits you. Your story matters! (@ucd_oa)



© Some rights reserved. For more information

Estimation of transitory changes in bending stiffness using the Hilbert-Huang transform

A. González & H. Aied

School of Civil Engineering, University College Dublin, Dublin, Ireland

ABSTRACT: A finite element model of a bridge can be calibrated based on field measurements, and then updated periodically using a structural health monitoring system. The value of a structural parameter such as bending stiffness can be adjusted to measurements using well-known modal updating techniques and monitored in conjunction with external effects such as temperature to assess the condition of the structure. A value of the parameter that is predominant during the period under investigation will be captured, however, in the case of bending stiffness, brief and transitory values could take place as a result of a section exceeding the yield point due to a moving traffic load. Given that the latter is probably the prelude of more severe damage, this paper proposes a novel two-stage method based on the Hilbert-Huang transform combined with a statistical optimization approach to characterize the stiffness changes associated with a non-linear response.

1 INTRODUCTION

1.1 *Non-linearity in the structural response*

Identification of damage or stiffness changes in a structure is mostly based on assuming a linear elastic response (Hester & González 2012, Lee 2009, Li et al. 2013, Nagarajaiah & Basu 2009). However, a section will only respond in a linear elastic range up to a certain yielding point beyond which a non-linear response will take over. How damage relates to non-linearity has been a subject of interest in recent research (Farrar et al. 2007). A non-linear behaviour is more likely in the case of deteriorated structures (i.e. corrosion or cracks in reinforced concrete structures) and/or large loads and deformations, although it can also be motivated by friction at the joints or presence of non-linear material, e.g. bearings (González & Aied 2015). In the case of damage due to corrosion, Stewart (2009) argues that losses of steel cross-sectional area can be of up to 16%, while Palsson & Mirza (2002) have found losses up to 80%. Clearly, this level of steel loss at a specific section can cause the moment-curvature relationship governing its response to exceed the linear elastic range and to enter a lower stiffness in a plastic range.

The unscented Kalman filter (Wu & Smyth 2007), the continuous wavelet transform (Hester & González 2012, Wang et al. 2013) and other methods (Chen et al. 2014, Kalvoda & Hwang 2010, Kijewski-Correa & Kareem 2006, Kunwar et al. 2013, Muto & Beck 2008, Nichols et al. 2010) have been examined for their applicability in characterization of non-linear responses and parameter identification. One of these methods is the Hilbert-Huang Transform (HHT), which has been used previously for a wide range of applications from ocean wave data to sound and climate variability (Huang et al. 1998, Huang & Pan 2006, Huang & Shen 2005).

1.2 *Application of the Hilbert-Huang transform to damage detection*

The HHT consists of: (1) splitting the original signal into a number of Intrinsic Mode Functions (IMFs) using a decomposition process, the so-called "Empirical Mode Decomposition" (EMD),

and (2) applying the Hilbert Transform (HT) to each IMFs to produce the Instantaneous Frequencies (IFs) (Kerschen et al. 2008). The HT by itself is used for mono-component signals (Feldman 1994, Frank Pai 2010) so the prior application of the EMD process is necessary to deal with multi-component signals. The application of the HHT to damage detection in linear structures has been shown to be able to detect and locate damage in beams and plates under transient loads (Kunwar et al. 2013, Quek et al. 2003, Roveri & Carcaterra 2012), although it appears to be sensitive to slight distortions in the signal. For instance, Yang et al (2003) assume a linear stiffness loss due to structural damage and using the HHT, they are able to show the location of damage and the change in frequency before and after damage via identification of a discontinuity in the instantaneous frequency. Kunwar et al (2013) apply the HHT to acceleration measurements from different locations in a damaged experimental bridge model and they find that sensors close to the damaged location detect the damage by a significant increase in the magnitude of the vibrations while sensors further away from the damaged location show little difference compared to the undamaged case even for very severe damage.

1.3 Objective

Unlike previous research aiming to capture fixed permanent damage from a linear response, this paper intends to identify and characterize brief stiffness changes once the yielding point is exceeded as a result of excessive loading at a section of a bridge due to a moving load. In particular, the structure is assumed to be a two-span continuous beam made of reinforced concrete where one of the sections follows a bilinear hysteresis model to simulate the post-yielding stiffness. Stiffness changes or crossings of the yielding point at this section can only be captured as they occur, given that once the section is unloaded, the linear elastic range will again govern the response. First, the post-yield stiffness loss in a selected section will be predicted using the IF (via the HHT) of the acceleration response at another section located in the mid-length of the first span. Once the non-linearity of an output response has been identified and localized via the HHT, the next logical step is to assess the stiffness loss associated with that non-linearity accurately, i.e. to quantify it. Finite Element (FE) updating methods have been commonly used to quantify linear and non-linear parameters of structures using accelerations and natural frequencies (Kalvoda & Hwant 2010, Mthembu et al. 2011), but this has never been done before for a structural change within a time frame as short as proposed here. Bayesian statistics (Earls 2013, Gelman et al. 2003, Marwala 2010, Mthembu et al. 2011) and cross-entropy (Dowling et al. 2012) are two statistical optimization methods that have been extensively used for model updating and stiffness characterization of structures. This paper tests the accuracy of both methods in estimating the post-yield to pre-yield ratio when a section yields. The issue to address is not so much the ability of these statistical methods in predicting structural parameters, something that has been demonstrated many times in the literature, but to test if the IFs can be used as a valid input to accurately predict instantaneous stiffness changes. Different values of post-yield stiffness and of the speed of the moving load are employed for this purpose.

2 SIMULATION MODEL

2.1 Bridge model

A scenario consisting of a continuous bridge made of two equal spans of 10 m each is modelled here using a beam discretized into 20 finite elements (Figure 1a). The modulus of elasticity is $E_c = 35 \times 10^9 \text{ N/m}^2$ and the material density is $\rho = 2400 \text{ kg/m}^3$. The cross-section is 12 m wide and 0.6 m deep, and it is assumed to be made of concrete and steel with equivalent inertia $I = 0.2753 \text{ m}^4$. The stiffness of each discretized element varies depending on the arrangement of reinforcement throughout the beam. Therefore, stiffness ratio is defined here as the ratio of the stiffness $(E_c I)_x$ for a particular element x to the stiffness of an undamaged element with double reinforcement $(E_c I)_0$. The hypothetical distribution of stiffness across the structure shown in Figure 1b is adopted to purposely introduce a variation of stiffness throughout the structure. For example, there is a stiffness ratio of 1 between 6 m and 8 m from the first support, and also between 12 m and 14 m, which correspond to two regions with both compressive and tensile reinforcement.

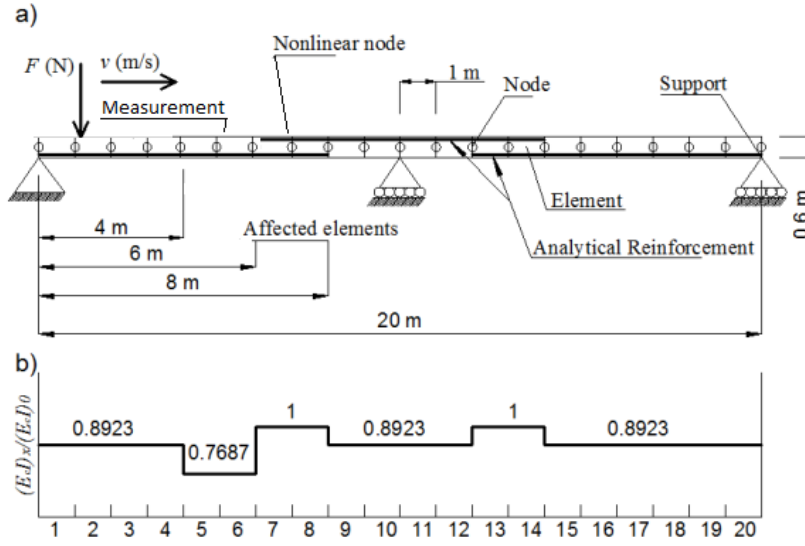


Figure 1. Beam model: (a) elevation and (b) stiffness ratio for each element.

In addition to sections with a stiffness ratio of 1, there are sections with a stiffness ratio of 0.8923, except for an artificially assumed weaker region of stiffness ratio 0.7687 between 4 m to 6 m. The reasoning behind this modelling is to test if a non-uniform distribution of stiffness could mislead the HHT in targeting a change in linear response.

The 20 discretized beam elements have two degrees-of-freedom (DOFs), namely vertical deflection $u_i(t)$ and rotation $\theta_i(t)$ at each end node i . The 4x4 elementary beam stiffness matrix ($[K_e]$) is given by Equation 1.

$$[K_e] = \begin{bmatrix} a & b & -a & b \\ b & c & -b & \frac{c}{2} \\ -a & -b & a & -b \\ b & \frac{c}{2} & -b & c \end{bmatrix} \quad (1)$$

where $a = 12E_c I_c / L_e^3$, $b = 6E_c I_c / L_e^2$, $c = 4E_c I_c / L_e$, and L_e is the length of the element ($L_e = 1$ m for the selected discretization level).

The moving load is modelled as a point force. The simple representation of the load used here is deemed to be sufficient to induce the desired effect of exceeding the yielding moment at a given section within a narrow time window. The equation of motion that governs the time-varying displacements (including vertical deflections and rotations for all nodes) $\{u(t)\}$, velocities $\{\dot{u}(t)\}$, and accelerations $\{\ddot{u}(t)\}$ due to the point force is given by:

$$[M]\{\ddot{u}(t)\} + [C]\{\dot{u}(t)\} + [K]\{u(t)\} = \{f(t)\} \quad (2)$$

where $[M]$, $[C]$, and $[K]$ are $n \times n$ global mass, damping and stiffness matrices respectively, being n the total number of DOFs of the system. Global matrices are formed by assembling elementary matrices taking common DOFs between elements into account. Viscous damping is typically low in bridges and the effect of $[C]$ is neglected in these simulations. The first four natural frequencies of the bridge model in the linear elastic range are 10.63, 16.38, 42.6 and 53.8 Hz. The applied point force moving at a velocity v (m/s) is represented by the time-varying vector $\{f(t)\}$ which contains the distribution of forces to the nodal DOFs of the structure. All values of $\{f(t)\}$ will be zero except those corresponding to the DOFs of the beam element where the load is applied. The moving load is distributed to the DOFs of the underlying element as a product of the Hermite shape functions. Equation 2 is implemented using the MATLAB programming language and solved based on the Wilson- θ integration method. The latter is uncondition-

ally stable if the acceleration is assumed to vary linearly within a specified extended time step τ , i.e. $\tau = r\Delta t$ where $r = 1.42$ and $\Delta t = 0.001$ s (Clough & Penzien 1993, Craig 1981, Nickel 1971).

2.2 Definition of non-linear elements

The post-yield behaviour of the two elements between 6 and 8 m is established by a stiffness curve different from that in the linear range. The transition between pre-yield and post-yield stiffness is typically smooth, but for simplification purposes, a bilinear model is employed here (Zeynalian et al. 2012). Figure 2 represents the assumed bilinear moment-curvature relationship. Moment M and curvature Φ are linear up to the elastic limit and also linear, although with a smaller slope (indicative of stiffness loss) in the plastic range. As a result, there is a sharp transition at the yielding point. M_y and Φ_y are the yield moment and yield curvature respectively. The value of the yield moment (M_y) is governed by the amount of steel reinforcement in the beam. The post-yield ratio, α in Figure 2, relates the pre-yield stiffness to the post-yield stiffness by $(E_c I)_p = \alpha (E_c I)_s$, where $(E_c I)_p$ is the post-yield stiffness and $(E_c I)_s$ is the stiffness of the undamaged section. Since a double reinforcement is assumed between 6 and 8 m (Figure 1a), the pre-yield stiffness $(E_c I)_s$ is equal to $(E_c I)_o$. Degradation, pinching, and permanent deformation are neglected (Pugasap 2006, Song & Der Kiureghian 2006, Stewart & Al-Harthi 2008), therefore this model may not necessarily be the most accurate, but acceptable for testing the ability in predicting stiffness changes when a section yields.

The bending moment, $M(t)$, at time instant t , is calculated at each section using the expression by Pinkaew & Asnachinda (2007):

$$M(t) = \left(\frac{(E_c I)_s}{L_e^3} \right) \times \left\{ \begin{matrix} (12\beta_j - 6L_e) & L_e(6\beta_j - 4L_e) & -(12\beta_j - 6L_e) & L_e(6\beta_j - 2L_e) \end{matrix} \right\} \times \begin{Bmatrix} u_i(t) \\ \theta_i(t) \\ u_{i+1}(t) \\ \theta_{i+1}(t) \end{Bmatrix} \quad (3)$$

where β_j is the location of the section within the element j where $M(t)$ is sought (i.e. $0 \leq \beta_j \leq L_e$), and $u_i(t)$, $u_{i+1}(t)$ and $\theta_i(t)$, $\theta_{i+1}(t)$ are vertical deflections and rotations respectively at both nodes of the element.

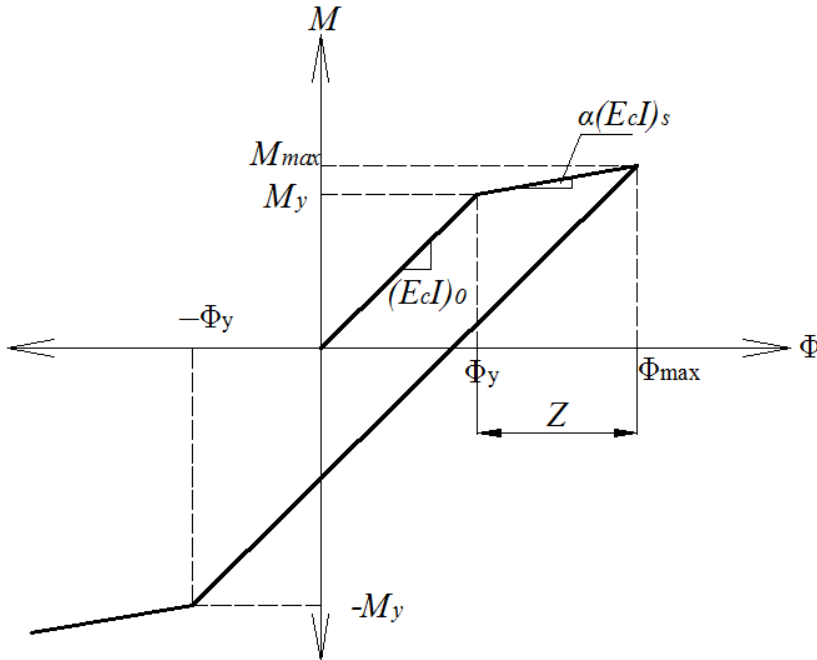


Figure 2. Bilinear hysteresis model of moment-curvature relationship.

If the bending moment $M(t)$ exceeds the yield bending moment (M_y), a hysteretic bending moment ($M_n(t)$) is introduced that is dependent on the hysteretic curvature ($Z(t)$). The hysteretic curvature ensures that the curvature at the non-linear elements does not return to its original value (i.e. $Z = \Phi_{\max} - \Phi_y$ in Figure 2) at unloading. The hysteretic moment, $M_n(t)$, is related to the bending moment, $M(t)$, indirectly through the yield curvature ($\Phi_y = M_y/(E_c I_s)$) and directly through the hysteretic curvature (Z) as defined by the equations that follow. The non-linear hysteretic moment ($M_n(t)$) is calculated using Equation 4 (Pinkaw & Asnachinda 2007, Pugasap 2006, Zeynalian et al. 2012):

$$M_n(t) = \alpha(E_c I)_p \Phi(t) + (1 - \alpha)(E_c I)_p Z(t) \quad (4)$$

where $Z(t)$ is the hysteretic curvature given by:

$$Z(t) = Z(t - 1) + \dot{Z}(t)\Delta t \quad (5)$$

and $\dot{Z}(t)$ is the incremental (i.e. derivative) hysteretic curvature, which is calculated using:

$$\dot{Z}(t) = \dot{\Phi}(t)[H_3(\dot{\Phi}(t)) \times H_4(Z(t - 1) - \Phi_y) + H_2(\dot{\Phi}(t)) \times H_1(Z(t - 1) + \Phi_y)] \quad (6)$$

where $\dot{\Phi}(t)$ is the derivative of the curvature with time and H_1 , H_2 , H_3 and H_4 are the Heaviside's step functions defined by Pugasap (2006) as:

$$\begin{aligned} H_1(\Phi) &= \begin{cases} 1, & \text{for } \Phi \geq 0 \\ 0, & \text{for } \Phi < 0 \end{cases} & H_2(\Phi) &= \begin{cases} 0, & \text{for } \Phi \geq 0 \\ 1, & \text{for } \Phi < 0 \end{cases} \\ H_3(\Phi) &= \begin{cases} 1, & \text{for } \Phi > 0 \\ 0, & \text{for } \Phi \leq 0 \end{cases} & H_4(\Phi) &= \begin{cases} 0, & \text{for } \Phi > 0 \\ 1, & \text{for } \Phi \leq 0 \end{cases} \end{aligned} \quad (7)$$

Equation 7 establishes if changes in the bending moment caused by the moving load represent a loading or an unloading event at the section under investigation. In order to allow for a post-yield stiffness behaviour of elements between 6 and 8 m into the dynamic response of Equation 2, the elemental stiffness matrices need to be recalculated at each point in time and the affected coefficients need to be updated accordingly in the global stiffness matrix. In the modelling process, the left node or right node of an element can be non-linear. In the case of both nodes being non-linear, then the stiffness matrix is simply the original stiffness matrix (undamaged element) (Equation 1) multiplied by the post-yield to pre-yield stiffness ratio α . In this simulation, it is assumed that yielding is localized at only one node, which coincides with the left-hand node of element 8 and the right-hand node of element 7. Therefore, the elemental stiffness matrices of elements 7 and 8 are given by Equations 8 and 9 respectively (Cheng 2000).

$$[K_{en1}] = \begin{bmatrix} \alpha a + qg & -ab & \alpha a + qg & -ab - qf \\ -ab & \alpha c & -ab & \alpha \frac{c}{2} \\ \alpha a + qg & -ab & \alpha a + qg & -ab - qf \\ -ab - qf & \alpha \frac{c}{2} & -ab - qf & \alpha c + qe \end{bmatrix} \quad (8)$$

$$[K_{en2}] = \begin{bmatrix} \alpha a + qg & -ab - qf & \alpha a + qg & -ab \\ -ab - qf & \alpha c + qe & -ab - qf & \alpha \frac{c}{2} \\ \alpha a + qg & -ab - qf & \alpha a + qg & -ab \\ -ab & \alpha \frac{c}{2} & -ab & \alpha c \end{bmatrix} \quad (9)$$

where q is given by $q = 1 - \alpha$, $e = 3E_c I / L_e$, $f = 3E_c I / L_e^2$ and $g = 3E_c I / L_e^3$. Other variables in the equations above have been defined before.

In summary, vertical deflections and rotations, their velocities and accelerations for all nodes of a two-span continuous FE beam traversed by a moving load are obtained via integration of Equation 2. The relative stiffness distribution with respect to the two-layer reinforcement,

shown for each element in Figure 1b, is employed to fill up the values of $E_c I$ populating the elementary stiffness matrices ($[K_e]$ defined in Equation 1), which are assembled into the global stiffness matrix $[K]$ of Equation 2. Those accelerations at mid-length of the first span (5 m from the first support, i.e. at the right node of element numbered 5 in Figure 1b) are then used in the following sections for characterizing the stiffness of the system using the HHT and model updating methods. The moment, $M(t)$, at any section within a discretized element and point in time t , can be calculated replacing vertical deflections and rotations of the two closest nodes into Equation 3. In this process, if the moment applied to a section, $M(t)$, exceeds the yield moment, M_y , at some instant during the crossing of the load, then, the non-linear elemental stiffness matrices defined in Equations 8 and 9 replace the matrix of the healthy elements defined in Equation 1 affected by the yielding of the section. More specifically, the yielding moment of the section at 7 m from the first support (i.e. right node of element numbered 7 in Figure 1b) has been purposely reduced to simulate a damaged section and to induce yielding as a result of the moving load. When the latter occurs, the elementary stiffness matrices of the elements numbered 7 and 8 in Figure 1b, typically represented by $[K_e]$ (Equation 1), are replaced by the two non-linear elemental stiffness matrices $[K_{en1}]$ (Equation 8) and $[K_{en2}]$ (Equation 9) at elements 7 and 8 respectively to allow for a post-yielding behaviour. The response of the section in the plastic range typically lasts only a small time interval (when the response follows the slope $\alpha E_c I$ in Figure 2), after which, the section is unloaded (i.e. the moment $M(t)$ decreases) and the matrixes of the healthy elements are reintroduced (i.e. the slope $E_c I$ governs the response again). The method proposed to estimate α from the simulated accelerations at this precise time interval is described next.

3 ALGORITHM FOR IDENTIFYING BRIEF STIFFNESS CHANGES IN NON-LINEAR STRUCTURAL SYSTEMS

This paper proposes a two-stage algorithm to characterize changes in structural stiffness as a result of a non-linear response. The algorithm estimates the level of post-yielding stiffness experienced by a section as it occurs during the load crossing by (1) applying the HHT to the acceleration response which allows identifying its occurrence and the instantaneous frequencies associated with this transitory situation, and (2) using a statistical optimization method which allows quantifying the stiffness loss corresponding to those instantaneous frequencies.

3.1 Calculation of frequencies by the Hilbert-Huang transform

The HHT (Chen et al. 2014, González & Aied 2015, Huang et al. 1998, Huang & Shen 2005, Huang & Pan 2006, Kerschen et al. 2008, Kunwar et al. 2013, Quek et al. 2003, Yang et al. 2003) is a data analysis method used for non-linear and non-stationary signals that consists of two main steps: the EMD, and the HT. The EMD is used to generate a collection of IMFs. An IMF is a component of the signal that satisfies two conditions: (1) The number of extrema and the number of zero-crossings must differ by no more than one, and (2) the mean value of the envelope defined by the maxima and the minima at any given time must be zero. The process of decomposing the signal into IMFs is done via a ‘sifting’ process as follows.

- First iteration:
 - a) Envelopes of local maxima and local minima of the signal are identified and created using a cubic spline interpolation scheme
 - b) The mean $m_1(t)$ of the upper and lower envelopes is calculated for each point in time
 - c) The difference between the signal and the mean, i.e. $h_1(t) = x(t) - m_1(t)$ is obtained. $h_1(t)$ rarely satisfies the two conditions of IMFs mentioned above and therefore, the process is repeated in a second iteration and likely more iterations as follows:
- Second and subsequent iterations: The steps a) to c) above are carried out again, only that this time $h_1(t)$ is treated as the signal. Step b) will produce a mean $m_{11}(t)$ and step c) will result in a signal $h_{11}(t) = h_1(t) - m_{11}(t)$. It is checked if $h_{11}(t)$ meets the two conditions for an IMF. If they are not met, the sifting process is repeated in a similar fashion, but with $h_{11}(t)$ being treated as the signal. After the sifting process is repeated k times, both conditions will actually be met and an IMF, i.e. $h_{1k}(t)$, will be obtained.

$$h_{1k}(t) = h_{1k-1}(t) - m_{1k}(t) \quad (10)$$

$h_{1k}(t)$ is treated as the first IMF, and the difference between the rest of the signal and the first IMF gives the residual $r_1(t) = x(t) - h_{1k}(t)$. This residual is used as the input to calculate the second IMF using the same iterative 'sifting' process described above. As before, the criterion for the sifting process to stop and define a second IMF is based on meeting the two conditions for an IMF. The decomposition process into IMFs is repeated S times until the value of $r_s(t)$ becomes a monotonic component from which no more IMFs can be extracted.

The second step of the HHT analysis is the application of the HT to the IMFs from which the Instantaneous Phase (IP), IF and amplitude of each IMF are calculated. A complex analytical signal, $z_i(t)$, is formed for each IMF consisting of a real part defined as the i^{th} IMF ($c_i(t)$), and an imaginary part defined by the HT ($y_i(t)$), that can be formulated in an exponential format as per Equation 11.

$$z_i(t) = c_i(t) + jy_i(t) = a_i(t)e^{j\text{IP}_i(t)} \quad (11)$$

where $j = \sqrt{-1}$, $a_i(t)$ is the amplitude at time t , and $\text{IP}_i(t)$ is the instantaneous phase. In other words, the analytical signal $z_i(t)$ represents a rotation in the complex plane with the instantaneous phase angle $\text{IP}_i(t)$ and the radius of rotation $a_i(t)$ given by Equations 12 and 13 respectively.

$$\text{IP}_i(t) = \arctan\left\{\frac{y_i(t)}{c_i(t)}\right\} \quad (12)$$

$$a_i(t) = \sqrt{|c_i(t)|^2 + |y_i(t)|^2} \quad (13)$$

Equation 14 obtains the instantaneous frequency $\text{IF}_i(t)$ associated with the i^{th} IMF at time t from the derivative of the instantaneous phase.

$$\text{IF}_i(t) = \frac{d}{dt}(\text{IP}_i(t)) \quad (14)$$

The final result of the HHT is an energy-frequency-time representation of the original data that allows characterizing the frequency of a nonlinear system.

3.2 Statistical optimization method

Statistical methods have been widely used for damage detection, parameter estimation and model updating (Mthembu et al. 2011). They are particularly suited to problems with limited information on the structure (as is usually the case) and lots of potential solutions available to fit the data. In these problems, they are useful in the sense that they give not only an estimation of the values of structural parameters but also of the confidence associated with this estimation. For the problem in hand, which deals with the identification of the post-yield to pre-yield stiffness ratio at a selected section, the theoretical model j with the value α that minimizes the objective function O_j given by Equation 15 is sought.

$$O_j = \sum_{i=t_0}^{t_0+N_{IF}\Delta t} (\text{IF}_{r,i} - \text{IF}_{t,i}(\alpha))^2 \quad (15)$$

where $\text{IF}_{r,i}$ and $\text{IF}_{t,i}(\alpha)$ are the instantaneous frequencies at the time instant i corresponding to the 'experimental/real' data and to the theoretical model with an assumed α (value to be quantified) respectively. In this objective function, t_0 is the time instant where calculations start, Δt is the time step between consecutive IFs and N_{IF} is the number of IFs considered in the calculation. All values in Equation 15 refer to a specific IMF. In this optimization problem, the only unknown is α . Clearly, such a problem could be solved by Monte-Carlo simulation, sampling a wide range of values of α and choosing the value giving the lowest objective function. However, the latter is not computationally efficient, particularly when applied to more complex models than the simple planar model tested in this paper. For this reason, the ability of two alternative statistical optimization methods, cross-entropy and Bayesian statistics, in estimating α is tested here. The following subsections describe how these methods can be implemented within the

context of Section 2, although they could be readily generalized to other scenarios with more than one unknown parameter.

3.2.1 Cross-entropy

Cross-entropy (Dowling et al. 2012, González et al. 2013) is an iterative optimization procedure that minimizes differences between measurements and the response by a theoretical model via an iterative procedure characterized by the generation of many trial structural models (beams, in this case) with the same geometry as the original structure but different mechanical properties. Initially, statistical distributions are assumed for each unknown structural parameter based on typical values. Trial beam models are then generated by randomly sampling from these statistical distributions. The value of an objective function that calculates differences between measurements and theoretical predictions is calculated for each trial beam. Then, the values of the structural parameters in the trial beams performing best (i.e. giving lowest values of the objective function) are used to update the statistical distributions and the process is repeated until convergence is achieved or the error of the objective function stops decreasing any further. For the problem in hand, it is sought to find the value of α leading to a response of the theoretical beam model that will resemble the IFs calculated from the simulated acceleration. Therefore, the objective function is defined by Equation 15. The entire process of quantifying the stiffness change using cross-entropy is illustrated in Figure 3 in which σ_b is the standard deviation at iteration b .

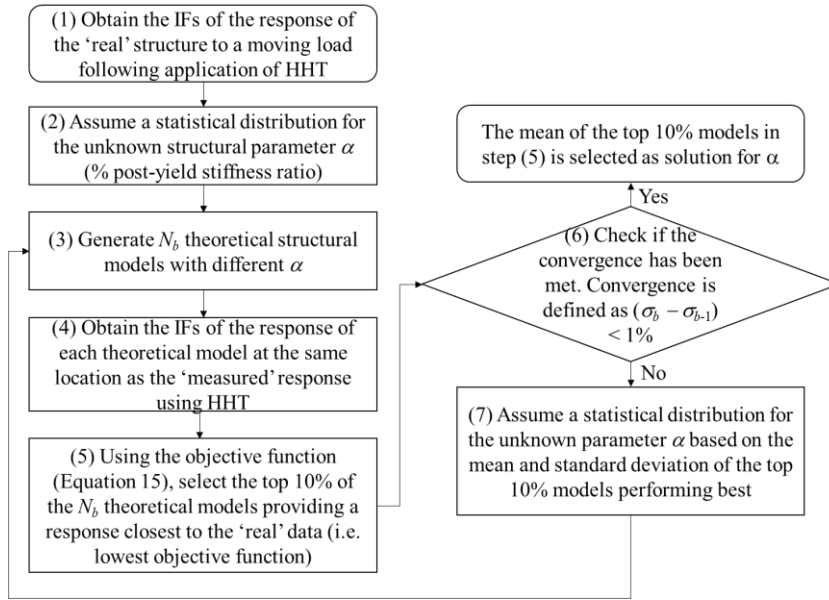


Figure 3. Schematic of the HHT combined with the cross-entropy optimization process.

3.2.2 Bayesian model updating

Scientific experimental or observational results generally consist of many sets of data of the general form $D = \{x_1, \dots, x_n\}$, where the x 's are homogeneous and possibly multi-dimensional observations. A central problem of any statistical analysis is the specification of a probability model which is assumed to describe the mechanism which has generated the observed data D as a function of a parameter vector θ (i.e. a single parameter α). The main consequence of these foundations is the mathematical need to describe by means of probability distributions for all uncertainties present in the problem. This task becomes more difficult when the system is non-linear. Unknown parameters in probability models must have a joint probability distribution which describes the available information about their values; this is often regarded as the characteristic element of a Bayesian approach. In Bayesian statistics, a set of measured data, D , for a specific model class M is used to assess the plausibility of the generated models depending on

the parameter value θ (Neal 1993). For this purpose, Bayes' theorem is applied. For the non-linear damage identification scenario under investigation, the observed data are taken as the instantaneous frequencies ($IF_{r,i}$, in which r is for 'real' between times $i = t_0$ and $i = t_0 + N_{IF}\Delta t$) obtained by applying the HHT to the acceleration signal at mid-length of the first span. The unknown parameter is the post-yield to pre-yield stiffness ratio, α . There are instantaneous frequencies for each IMF. Here, the IMF that appears to be more sensitive to changes without the interference of other frequency components is selected as the 'experimental/real' data.

One contrast between conventional statistics and the Bayesian approach is that parameters are treated as random variables within the Bayesian theory. This is not a description of their variability but a description of the uncertainty about their true values. A Bayesian analysis synthesizes both sample data (IF_r), expressed as the likelihood function ($P_L(IF_r|\alpha)$), and the prior distribution ($P_r(\alpha)$), which represents additional information that is available. The posterior distribution ($P_o(\alpha|IF_r)$) expresses what is known about a set of parameters (in this case, the unknown parameter is α) based on both the sample data and prior information. A fundamental feature of the Bayesian approach to statistics is the use of prior information in addition to the 'experimental/real' data. The prior information is represented by a distribution giving the probability that α took any particular value based on whatever additional information is given. Bayes's theorem, synthesizing these two sources of information, is applied through Equation 16.

$$P_o(\alpha|IF_r) \propto P_r(\alpha)P_L(IF_r|\alpha) \quad (16)$$

The proportionality symbol \propto expresses the fact that the product of the likelihood function and the prior distribution on the right-hand side of Equation 16 must be scaled (sum of probability must equal to one) to integrate to one over the range of plausible α values to be a proper probability distribution. The scaled distribution $P_o(\alpha|IF_r)$ is the posterior distribution for α given the data IF_r . The posterior distribution expresses what is now known about α based on both the sample data (likelihood) and the prior information. One way to scale the posterior distribution is dividing by what is known as the evidence ($P(IF_r)$):

$$P_o(\alpha|IF_r) = \frac{P_r(\alpha)P_L(IF_r|\alpha)}{P(IF_r)} \quad (17)$$

where $P_o(\alpha|IF_r)$ is the posterior probability of the parameter given the 'experimental/real' data IF_r and $P_r(\alpha)$ is the probability of prior distribution of the parameter α . The prior distribution function contains information that is known about the problem. In this paper, the prior distribution is assumed to be Gaussian (Neal 1993):

$$P_r(\alpha) \sim N(0, \sigma^2) \quad (18)$$

The Gaussian prior has been successfully used to identify a large number of weights in neural networks (Gelman et al. 2003, Marwala 2010) and therefore it is assumed that will also be valid for the identification of the single updating parameter in this investigation.

The likelihood function can be defined as the probability of observing the data IF_r being conditional on the values of the parameter α . Initially, the parameter α is set arbitrarily and the response of the theoretical model is generated. The predicted response at some location along with the structure, $IF_{t,i}(\alpha)$, will differ from the 'experimental/real' data, $IF_{r,i}$, by some amount at instant i . The experimental data is simply the predicted response plus some amount of error at each time step. If the error between the predicted and 'experimental/real' data is assumed to follow a Gaussian distribution, then the probability that the 'experimental/real' data is produced by the generated model, under assumed parameter (α) and some variance (σ) is:

$$P_L(IF_{r,i}|\alpha) = \frac{1}{(\sqrt{2\pi}\sigma^2)^{N_{IF}}} \exp \left[-\frac{1}{2\sigma^2} \sum_{i=t_0}^{t_0+N_{IF}\Delta t} \left(\frac{IF_{r,i} - IF_{t,i}(\alpha)}{IF_{r,i}} \right)^2 \right] \quad (19)$$

From the above, it can be stated that the probability of $IF_{r,i}$ is conditional on the parameter α and variance σ , the so-called likelihood probability. The likelihood function along with Equation 18 is used to obtain the posterior distribution ($P_o(\alpha|IF_{r,i})$) at instant i . In Equation 17, $P(IF_r)$ is the evidence or marginal likelihood which is a normalized constant that does not depend on or affects the shape of the posterior distribution. The analytical evaluation of $P(IF_r)$

may be difficult or impossible if the product of the prior and the likelihood is not simple (usually a multi-dimensional Gaussian distribution). Therefore, the resulting posterior distribution is not well-behaved, i.e. the integration of the posterior distribution does not add to one. A problem associated with a statistical approach such as Bayesian statistics is that posterior distributions are almost always unknown due to the variability and complexity of the parameters to be updated. Sampling from the posterior distribution is difficult and sometimes impossible without the use of Markov Chain Monte Carlo (MCMC) sampling methods. Nichols et al (2011) apply a new method of MCMC, i.e. the Metropolis-Hastings (MH) algorithm, to sample from a posterior distribution and identify a crack location, its length and orientation. Nichols et al (2010) identify linear and non-linear parameters in a Multi-Degree-of-Freedom structure with the MH algorithm to sample from the posterior distribution in a Bayesian approach, and they are also able to locate and quantify (size and depth) the level of delamination in a composite beam.

In this paper, the use of such evidence in Bayes's theorem is excluded by, first, dividing Equation 17 by the sum of the prior probability times the likelihood probability instead of the use of the term $P(IF_{r,i})$, leading to:

$$P_o(\alpha|IF_r) = \frac{P_r(\alpha)P_L(IF_r|\alpha)}{\sum_1^{N_b}(P_r(\alpha)P_L(IF_r|\alpha))} \quad (20)$$

In the equation above, N_b is the number of generated beams with different parameter values (α 's) and these parameters values are extracted from the prior distribution. So initially Bayes' theorem is used to obtain a posterior distribution of the data assuming it is a Gaussian distribution. Once the posterior distribution is obtained, it is used as the prior distribution in the next iteration if the number of iterations (N_i) is not exceeded. The process is repeated until the variance σ is sufficiently small and no further iterations are required as the difference of the parameter between consecutive iterations becomes negligible or very small.

Secondly, the use of Equation 17 without using evidence does not give a probability distribution (i.e. prior distribution \times likelihood distribution > 1), therefore a sampling technique is used to sample from the posterior distribution $P_o(\alpha|IF_{r,i})$ to ensure that the posterior distribution is a probability distribution. Sampling techniques are useful numerical methods which can be used to simplify the process of Bayesian inference by proposing a set of random samples from a posterior distribution. Therefore, sampling techniques are employed to predict the updating parameter distribution. Although there are different sampling techniques applied in the literature (Mthembu et al. 2011, Neal 1993), the MH algorithm is chosen here due to its general, powerful and easy implementation. The algorithm constructs a Markov-Chain but does not care about the full conditionals. Figure 4 shows the full process of the approach.

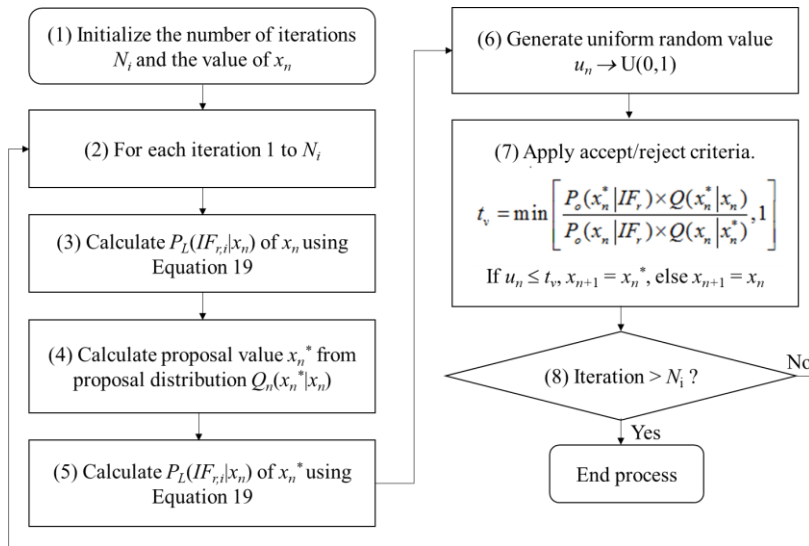


Figure 4. Schematic of the HHT combined with Bayesian updating process.

The main aim of the MH algorithm is to generate dependent samples of parameter estimates that fall in the posterior distribution ($P_o(\alpha|I F_r)$). By letting $\alpha = x_n$ (where $n = 1 \dots N_i$, being N_i the number of iterations) as the current value, it is possible to obtain x_{n+1} . The first stage of the MH process is to generate a proposal value (x_n^*) from a proposal distribution ($Q(x_n^*|x_n)$). The proposal distribution is normally chosen as a Gaussian distribution with a mean x_n and variance σ . x_n^* is either rejected or accepted depending on the acceptance criterion as per Figure 4. The iteration procedure produces N_i dependent samples of x_n from an unknown posterior distribution.

Points made in favor of the Bayesian approach argue that it offers an intuitive and meaningful approach to analyzing uncertainty, that it gives the ability to tackle more complex problems and that it allows the incorporation of prior information in addition to the ‘experimental/real’ data. While classical frequentist approaches do not provide an interval estimate containing the true value of the parameter, the Bayesian approach allows the construction of interval estimates which do have a probabilistic interpretation. There is controversy with regard to defining the prior distribution. A way to represent prior information is to specify skeptical prior distributions (which is the case of this paper using Gaussian distribution). In doing so, the idea of selecting a non-informative prior fails to exploit the full potential of the Bayesian approach. However, there is no unique way in which the prior distribution is defined without a high level of uncertainty.

4 THEORETICAL TESTING

This section assumes that the stiffness distribution of the structure in its linear form, i.e. the stiffness profile and the boundary conditions of Figure 1 are available. This stiffness distribution can be obtained via the application of modal updating techniques based on measurements in free vibration of the structure as demonstrated by Mthembu et al (2011). It is also assumed that the magnitude and speed of the moving load are known. In practice, these values can be obtained from a weigh-in-motion system installed prior to the bridge. Therefore, this section places focus upon the identification of stiffness changes of short duration as a result of yielding during forced vibration. The relevance of this investigation lays on the possibility of identifying those sections that yield more often, and consequently, are weakened and closer to the failure point. This information can be used to prioritize those bridges (and bridge sections) requiring immediate attention. It is acknowledged that the simulated test conditions here are rather ideal. In a real-life situation, there will be inaccuracies in the estimates provided by the HHT-statistical optimization process derived from the uncertainty associated with noise and parameters assumed for the load and the theoretical FE model.

4.1 Identification of stiffness loss after yielding using HHT

The response at mid-length of the 1st span (i.e. at a section located 5 m away from first support) of a 20 m long two-span continuous beam (as described in Section 2) is obtained when traversed by a load of 100 kN moving at 15 m/s. Figure 5 shows the acceleration for a scenario where the beam has not reached its yielding point yet. In this figure, the horizontal axis gives the time from the instant the load enters the bridge. Therefore, the load will be over the measurement section at 0.333 s and over the internal support at 0.667 s. Free vibration starts at 1.33 s.

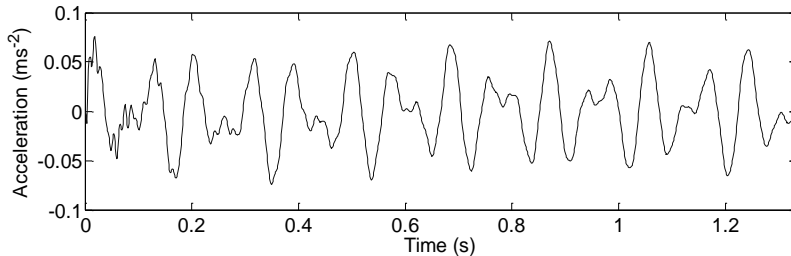


Figure 5. Acceleration at mid-length of the first span due to a load moving at 15 m/s without yielding.

The IMFs and IFs of the acceleration response in Figure 5 are shown in Figures 6 and 7 respectively. For each IMF, IFs (Equation 14), represented by dots in Figure 7, vary with time, even though the stiffness and mass matrices of the system remain constant. This is a consequence of the influence of the static component of the response and mode mixing in the EMD process. IMFs separate high and low-frequency components, with IMF1 containing the highest frequencies of the signal. IMF3 and IMF2 give the closest IF to the actual first (i.e. 10.63 Hz) and 2nd (i.e. 16.38 Hz) natural frequencies of the structure respectively. Mode mixing between consecutive IMFs is evident, especially between IMF1 and IMF2. In the case of IMF1, IFs have values close to 100 Hz between 0 and 0.2 s, and around the 4th and 3rd natural frequencies (i.e. 53.8 and 42.6 Hz) between 0.2 and 0.6 s, and they drop to the 2nd natural frequency after 0.6 s. Mode mixing associated with EMD has been mitigated to some extent by the development of techniques such as Ensemble Empirical Mode Decomposition (Aied et al. 2016, Wu & Huang 2009).

Figures 5, 6 and 7 correspond to a linear system where the frequencies of the system remain constant during the load crossing (mass of the vehicle is assumed to be negligible compared to the bridge mass here). When the yield bending moment, M_y , is exceeded (Figure 2), the response of the beam becomes non-linear, and the stiffness matrix must be adjusted as described in Section 2.2. If a loss in reinforcement (e.g. reduced steel cross-sectional area due to corrosion) is assumed between 6 and 8 m (Figure 1a), the value of M_y will be lower than that corresponding to an intact steel section (Nickel 1993). In particular, the yield moment M_y in this hypothetical corroded region has been assumed to be 95% lower than the original intact steel section. This selection of M_y guarantees that the section at 7 m will yield before any other elements during the crossing of the moving load. Other combinations of load and yield moment could have also been employed to demonstrate the ability of the proposed algorithm in capturing and quantifying a sudden stiffness loss as it occurs.

The acceleration at mid-length of the first span is shown in Figure 8 when using $\alpha = 0.1$ for the yielding of the section at 7 m from the first support. The impact of post-yield stiffness on the acceleration response is evident after 0.3 s and 0.7 s during which $\alpha = 0.1$ is acting. The first signs of yielding developing at 0.3 s correspond to a location of the load at $0.3 \times 15 = 4.5$ m from the first support, that is, yielding for the section at 7 m occurs before the load reaches the location due to an acting moment that has already exceeded M_y . However, the impact and level of yielding are not clear from the acceleration response alone.

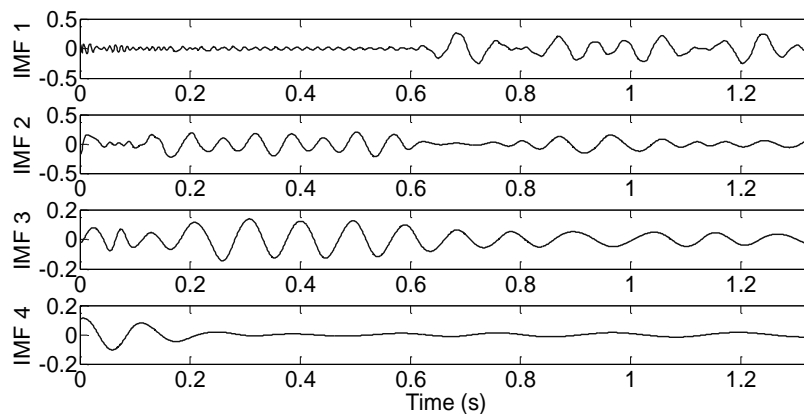


Figure 6. IMFs 1-4 of the acceleration at mid-length due to a load moving at 15 m/s without yielding.

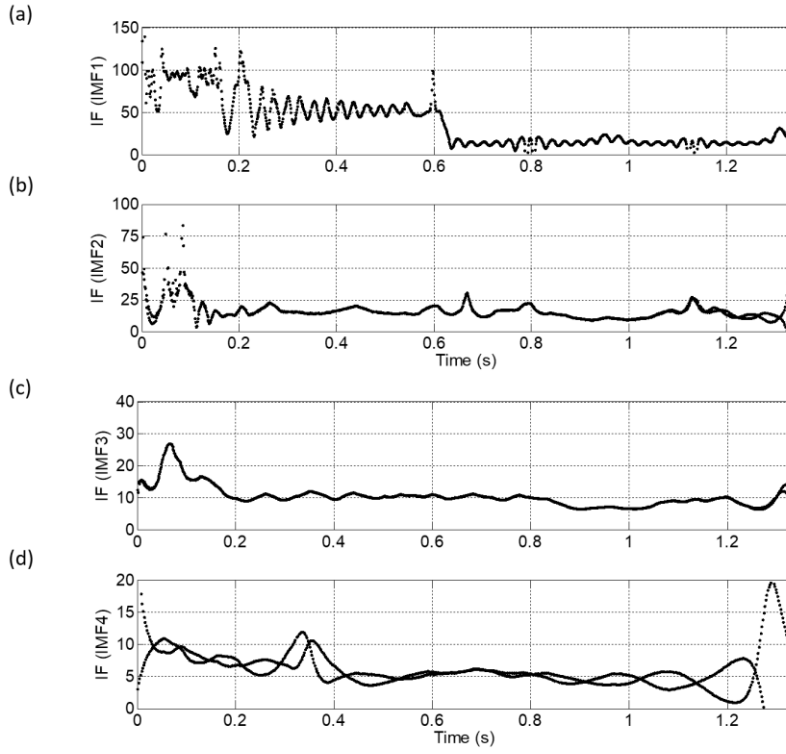


Figure 7. Instantaneous frequency of acceleration at mid-length of 1st span without yielding due to a load moving at 15 m/s for: (a) IMF1, (b) IMF2, (c) IMF3, and (d) IMF4.

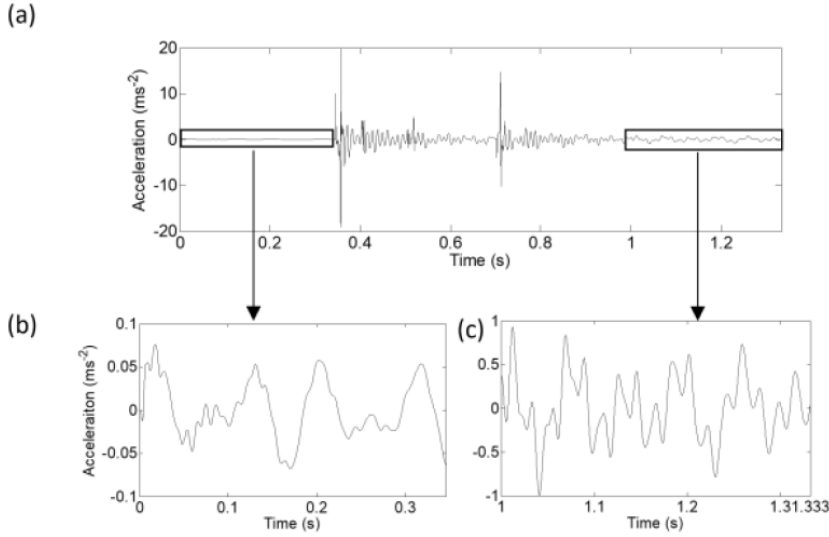


Figure 8. Acceleration at mid-length of the first span due to a load travelling at 15 m/s using $\alpha = 0.1$: (a) total response in forced vibration, (b) response before section at 7 m yields and enters the plastic range (0.35 s), and (c) response after section at 7 m re-enters the elastic range (0.9 s).

Figure 9 shows the IMFs 1-4 corresponding to the acceleration in Figure 8. There are sharp peaks around 0.35 s and again around 0.7 s. As previous research has shown using other structural models (Aied et al. 2016, Meredith et al. 2012), these sharp peaks can be used to identify periods of stiffness changes (i.e. due to the presence of damage). The IFs of IMFs 1-4 are shown in Figure 10. As expected, the disturbances introduced by stiffness changes at the 7 m section, are also captured by the associated IFs in the form of sudden discontinuities.

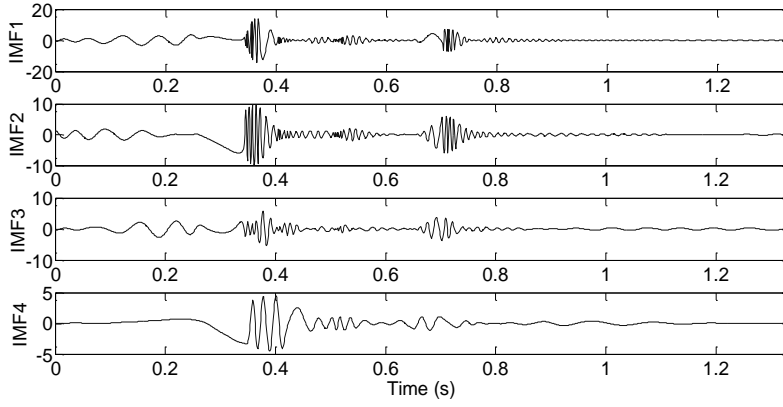


Figure 9. IMFs 1-4 of acceleration at mid-length due to a load travelling at 15 m/s using $\alpha = 0.1$.

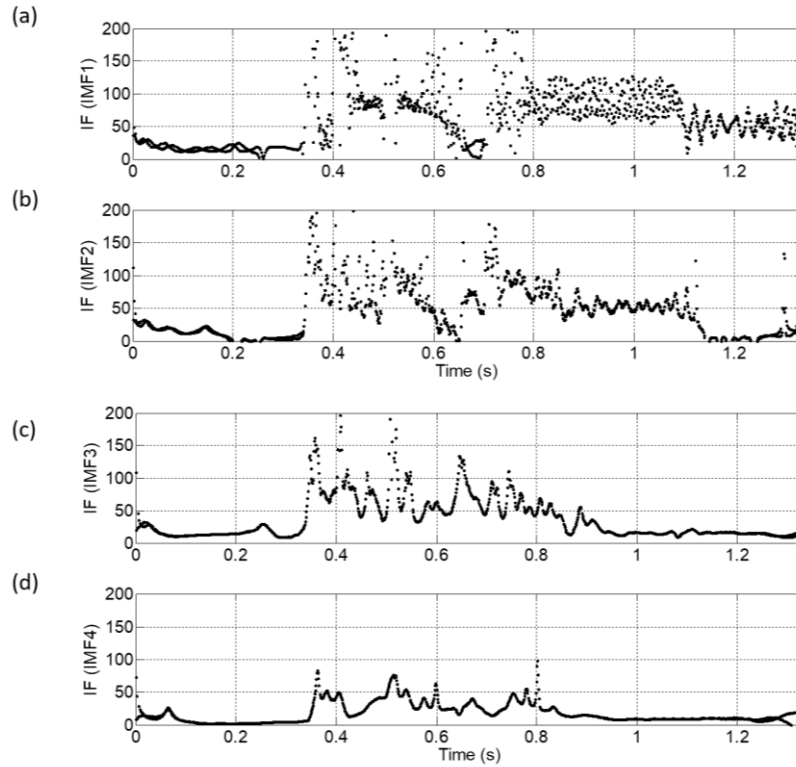


Figure 10. Instantaneous frequency of acceleration at mid-length of 1st span due to a load travelling at 15 m/s using $\alpha = 0.1$ for: (a) IMF1, (b) IMF2, (c) IMF3, and (d) IMF4.

Figure 11a shows the ‘real’ variation of stiffness with time using $\alpha = 0.1$ at the section under investigation and Figure 11b shows the IP of the acceleration signal in Figure 10a. Figure 11b has been calculated by applying Equation 12 and Figure 11a has been obtained following Section 2.2. The IP in Figure 11b captures the time instants of stiffness drop (i.e. post-yield stiffness) at 0.35 s and 0.7 s, but it is less clear when the stiffness drops at 0.41 s and 0.5 s. This is attributed to the duration of the stiffness drop, being longer at times 0.35 s and 0.7 s than at 0.41 and 0.5 s. At 0.5 s there are two consecutive drops in stiffness of shorter duration than other peaks. The derivative of the IP leads to the IF and as expected, post-yield stiffness in Figure 11b is denoted by a sudden change in slope (i.e. larger gradients in the phase) when yielding occurs.

In Figure 12, the IPs of IMF1 are calculated for two simulations with a load velocity of 5 m/s and two α values of 0.1 (large stiffness loss) and 0.8 (small stiffness loss). The ‘real’ stiffness change with time is shown in Figures 12a and 12c for $\alpha = 0.1$ and $\alpha = 0.8$ respectively.

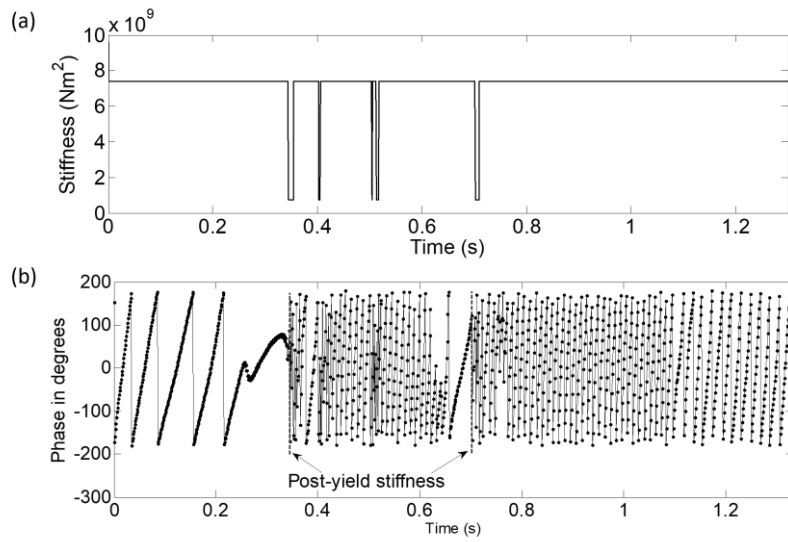


Figure 11. (a) Instantaneous stiffness and (b) Instantaneous phase associated with IMF1 of the acceleration at mid-length of 1st span due to a load travelling at 15 m/s using $\alpha = 0.1$.

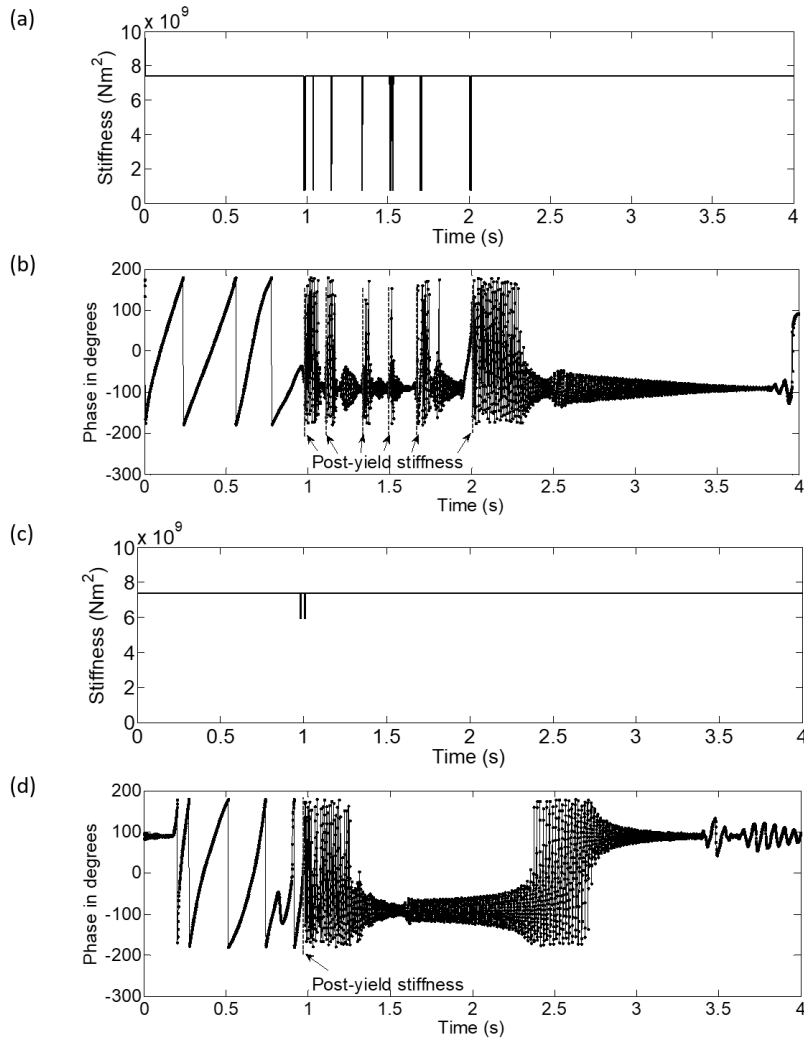


Figure 12. Instantaneous stiffness and instantaneous phase associated to IMF1 of the acceleration at mid-length of 1st span due to a load travelling at 5 m/s using $\alpha = 0.1$ in (a) and (b), and using $\alpha = 0.8$ in (c) and (d).

Stiffness changes can be identified more clearly in Figure 12b (lower speed) than in Figure 11b. The time duration of the drop in stiffness is almost instantaneous due to loading and unloading scenarios of the moving load. Figures 12b and 12d denote the time instances when post-yield stiffness starts to develop by large gradients at approximately 1 second. While Figure 12b is able to approximately resemble the pattern in Figure 12a after that initial instant, Figure 12d is unclear.

This section has demonstrated the capability of the HHT for identifying and localizing a non-linear response in time. IMFs, IFs and IPs have all left evidence of stiffness changes. As expected, this evidence has been clearer for the lowest speed and the lowest α . In order to quantify the post-yield stiffness, IFs are preferred as input for the updating methods in the next section on the basis of its physical meaning.

4.2 Quantification of post-yield stiffness using a statistical approach

The IF of acceleration extracted in Section 4.1 is used as input to cross-entropy and Bayesian statistical methods to identify the α value for the section at 7 m. In this procedure, it is important to choose the correct IMF. For the case of a load travelling at 15 m/s, IMF2 appears to be the most sensitive IMF to changes in stiffness. For instance, IMF1 exhibits higher interference of other frequency components than IMF2. There are obvious differences between the IFs associated with IMF2 for a response with $\alpha = 0.1$ (Figure 10b) and the IFs associated with IMF2 for a response without yielding (Figure 7b). In the procedure that aims to minimize the objective function defined by Equation 15, it is not necessary to choose the IFs for the entire duration of the load crossing, but only those IFs within a time interval where there are potential signs of initiation and decline of the post-yield stiffness loss effect. For $\alpha = 0.1$, the impact of loss in stiffness on IF of IMF2 can be visualized in Figure 13 between 0.35 s and 0.6 s, while between 0.8 s and 1.1 s the IF is close to the 4th natural frequency of the structure.

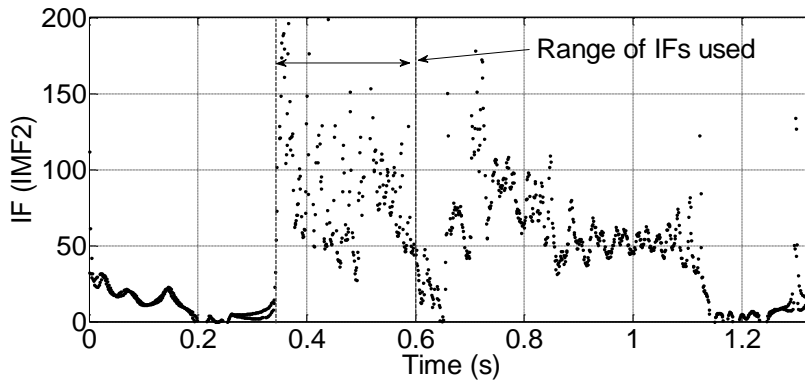


Figure 13. Range of IFs used in the optimization procedure.

Once the time interval from 0.35 s to 0.6 s has been established, α can be calculated by two alternative means: cross-entropy and Bayesian statistics described in Sections 3.2.1 and 3.2.2 respectively. The accuracy of cross-entropy and Bayesian estimations of α is illustrated by Figures 14 and 15 respectively, for three different levels of post-yield stiffness loss: $\alpha = 0.1$ (high stiffness loss in post-yielding), $\alpha = 0.2$ and $\alpha = 0.8$ (low stiffness loss in post-yielding). In all cases, Bayesian statistics and cross-entropy detect the value of α exactly with the exception of a small inaccuracy in the prediction of $\alpha = 0.8$ by cross-entropy (Figure 14c).

The parameters employed in the cross-entropy procedure are a total of 1000 trial beams generated in each iteration with an initially assumed normal distribution for α of mean 0.5 and standard deviation 0.5. The convergence criterion is established as the difference between standard deviations in consecutive iterations being less than 1%. It is interesting to note that the final distribution in Figure 14c associated with the inaccurate prediction of α has a wider standard deviation than the final narrow distributions in Figures 14a and 14b associated with exact predictions.

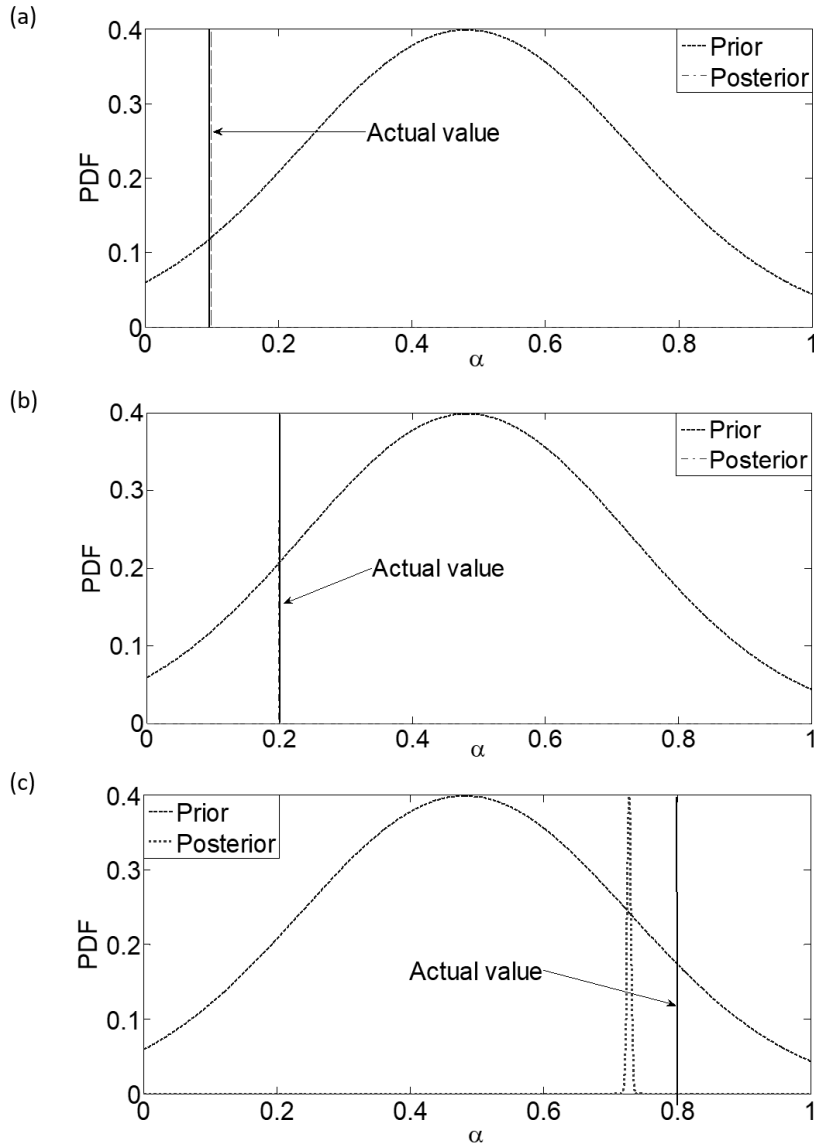


Figure 14. Cross-entropy method for identification of post-yield to pre-yield stiffness ratio using: (a) $\alpha = 0.1$, (b) $\alpha = 0.2$, and (c) $\alpha = 0.8$.

Bayesian statistics is founded on maximizing the likelihood function. From 1000 generated beams ($N_b = 1000$), the most likely value that fits the IFs is chosen and used as a prior probability and the process of Bayesian inference is repeated for the same beams until a value is reached with highest posterior probability. When 1000 beams are generated (with similar properties but different parameter α), their likelihoods (Equation 19) are assessed, and their posterior distribution is then calculated. The value with the highest posterior probability is used as the prior mean, while the variance is obtained from the values generated by the prior distribution. For example, at the 200th iteration, the posterior probability distribution may have a mean of 0.15 (if 'real' $\alpha = 0.1$) and variance of 0.2, which are used as the mean and variance for the prior distribution from which 1000 α 's are generated. This is repeated until the difference between consecutive standard deviations is minimal, i.e. smaller than 1%. The validity of this assumption is discussed further on using a sampling method. While the distributions using cross-entropy are plotted for the x-axis (α) from 0 to 1 in Figure 14, the posterior distributions using Bayesian analysis have a wider standard deviation and they are represented from -1 to 1 in Figure 15 for illustrative purposes. This is attributed to the variance associated with 1000 beams considered by Bayesian analysis in contrast to 100 beams (i.e. top 10%) considered by cross-entropy.

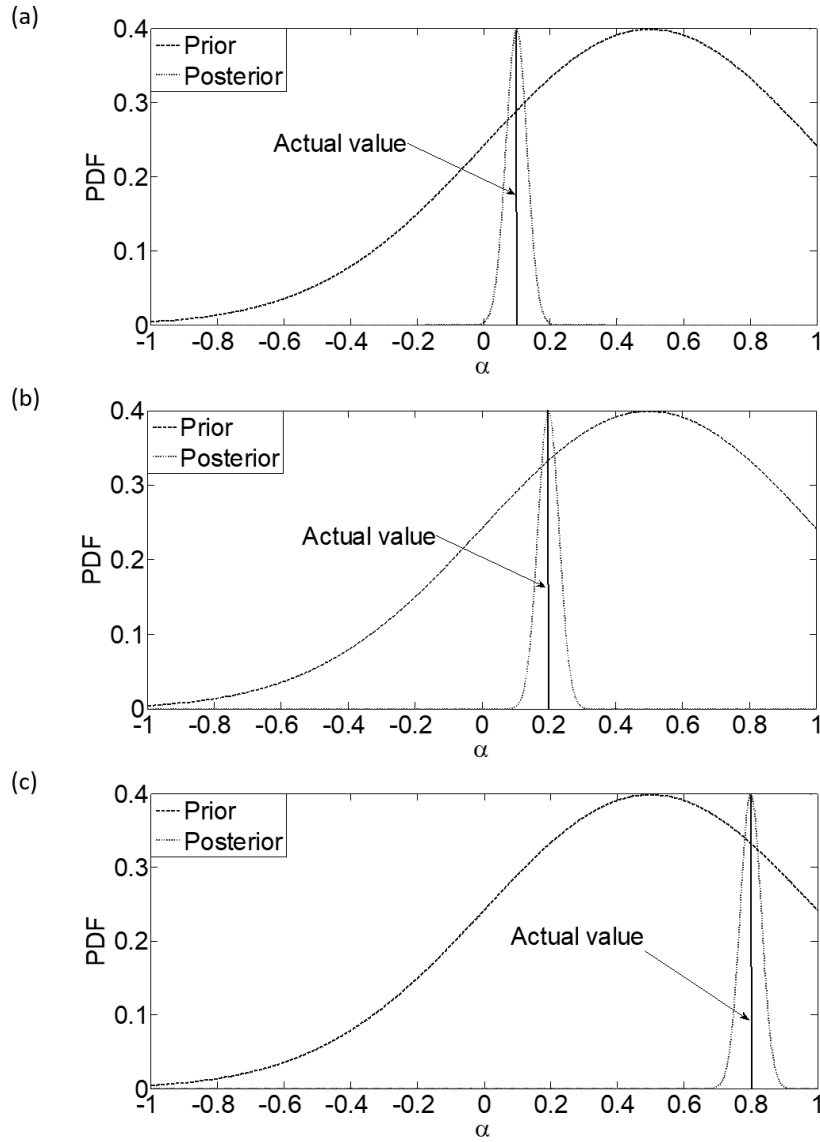


Figure 15. Bayesian statistics for identification of post-yield to pre-yield stiffness ratio using: (a) $\alpha = 0.1$, (b) $\alpha = 0.2$, and (c) $\alpha = 0.8$.

Table 1 provides errors in the estimation of α using Bayesian statistics, for a load speed of 15 m/s and different levels of post-yielding stiffness and iterations. Table 2 gives relative errors in the estimation of post-yielding stiffness using Bayesian statistics, for a value $\alpha = 0.1$ and different load speeds and iterations. In Tables 1 and 2, μ_{pr} and σ_{pr}^2 are the prior mean and variance while μ_{po} and σ_{po}^2 are the posterior mean and variance, respectively. These tables show that 1000 iterations lead to negligible errors and better results than 100 iterations.

Table 1. Mean and variance of the iteration process using Bayesian statistics for different α .

Actual value	Prior		100 iterations (posterior)			1000 iterations (posterior)		
α	μ_{pr}	σ_{pr}^2	μ_{po}	σ_{po}^2	%Error	μ_{po}	σ_{po}^2	%Error
0.1	0.5	0.5	0.0926	0.1	7.4	0.0986	0.0316	1.4
0.2	0.5	0.5	0.1907	0.1	4.65	0.1994	0.0316	0.3
0.8	0.5	0.5	0.7981	0.0704	0.24	0.8	0.0316	0

Table 2. Mean and variance of iteration process using Bayesian statistics, $\alpha = 0.1$ and different speeds.

$\alpha = 0.1$	Prior		100 iterations (posterior)			1000 iterations (posterior)		
Speed (m/s)	μ_{pr}	σ_{pr}^2	μ_{po}	σ_{po}^2	%Error	μ_{po}	σ_{po}^2	%Error
15	0.5	0.5	0.0926	0.1	7.4	0.0986	0.0316	1.4
25	0.5	0.5	0.2597	0.0987	159.7	0.1009	0.0316	0.9
35	0.5	0.5	0.0992	0.1	0.8	0.1002	0.0316	0.2

Section 3.2.2 explains that in Bayesian statistics, it is always difficult to obtain a well behaved posterior distribution of the data due to the properties of Bayes' theorem and the marginal likelihood function. In this paper, it is initially assumed that the posterior distribution is a normal distribution and the maximum likelihood function is used to calculate the parameter that fits the data best. The MCMC approach is applied using the MH algorithm to sample from an unknown posterior distribution. The sampled values have an initial value of μ_{po} (mean of the posterior distributions from Tables 1 and 2) and are plotted for true $\alpha = 0.1$ in Figure 16a and for true $\alpha = 0.8$ in Figure 17a. As discussed before, the sampled values do not correspond to any distribution. The frequencies of the values sampled from the posterior distribution are plotted in Figures 16b and 17b, where α values around 0.1 and 0.8 in Figure 16 and around 0.4, 0.5 and 0.8 in Figure 17 produce the highest number of acceptance rate.

Cross-entropy and Bayesian statistics have proven to estimate the post-yield stiffness to pre-yield stiffness ratio from the IFs successfully. The Bayesian approach has appeared to be more robust than cross-entropy, but the latter is simpler and easier to implement. Benefits of the Bayesian approach are its flexibility and possibility of integration with different sampling techniques such as MH algorithm and nested sampling. Regarding computational time, the Bayesian approach has performed faster, i.e. the cross-entropy simulations needed to find the solution in Figure 14a take around 2.5 hours for 1000 generated beams ($N_b = 1000$) compared to the Bayesian simulations for 1000 iterations taking between 1 and 2 hours, based on a HP Intel Core i7 windows system with 3.5 GHz RAM and 64-bit operating system.

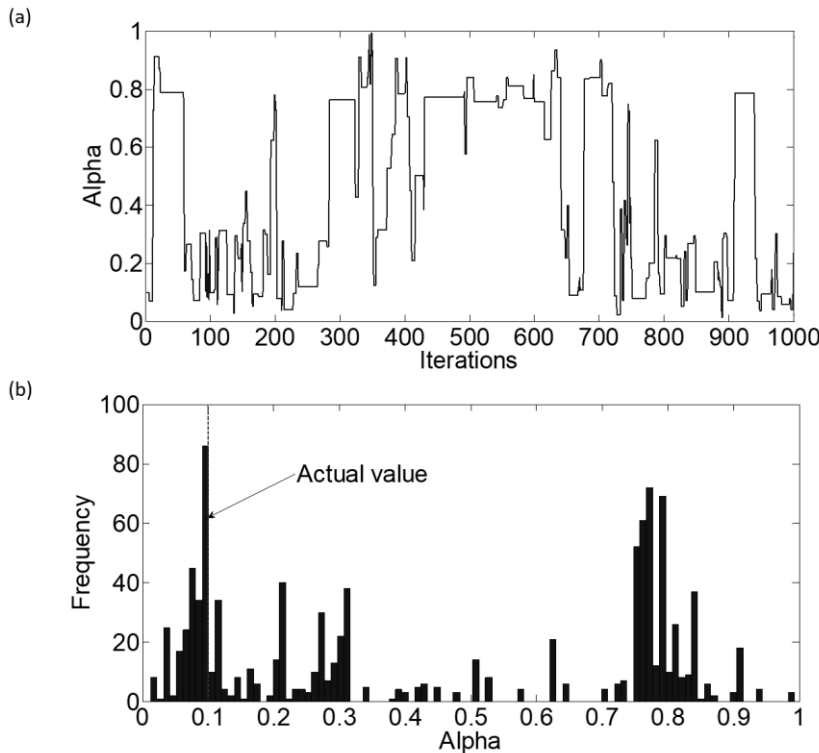


Figure 16. Sampled values of α from the posterior distribution at 15 m/s seeking for true $\alpha = 0.1$: (a) sampled value at each iteration and (b) frequency of α after 1000 iterations.

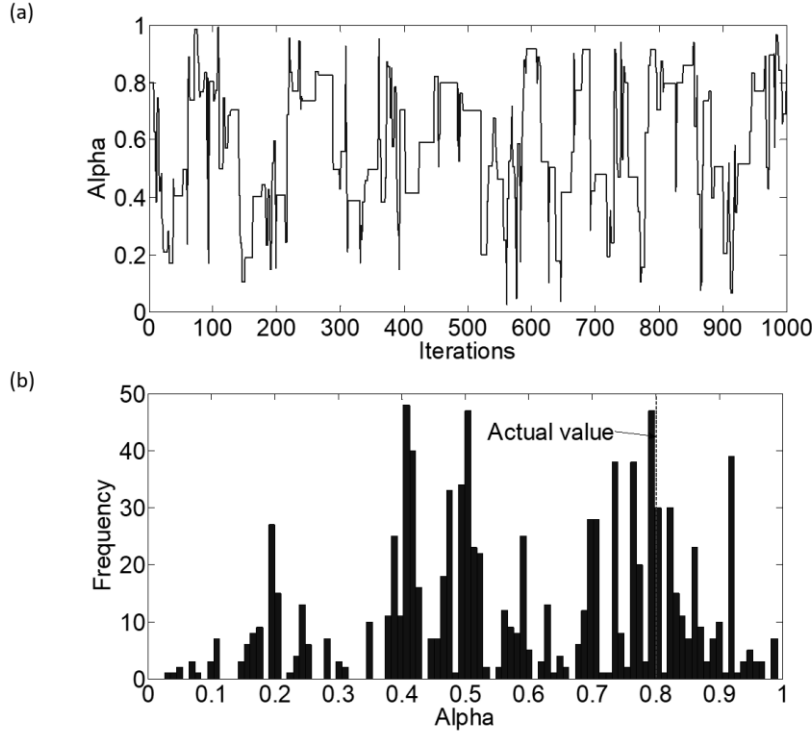


Figure 17. Sampled values of α from the posterior distribution at 15 m/s seeking for true $\alpha = 0.8$: (a) sampled value at each iteration and (b) frequency of α after 1000 iterations.

5 CONCLUSIONS

A reasonably accurate FE model of a structure can be calibrated via field testing. Then, vibration measurements will be compared against the model periodically to identify permanent stiffness changes. However, there are other types of stiffness changes that are only transitory and of very short duration, i.e. those due to yielding. The identification of these short-duration changes can be important to ensure the safety of the structure, i.e. by identifying those sections more sensitive to changes and as a result, to failure. For that purpose, this paper has proposed a mathematical procedure that predicts the level of post-yield stiffness loss in a bilinear damaged continuous beam using a two-stage process. In the first stage, the HHT has been applied to the acceleration response to calculate the associated instantaneous frequency response and to locate the period at which changes in stiffness take place. Sudden stiffness changes have been revealed in three types of outputs of the HHT: (i) as sharp peaks in the intrinsic mode functions, (ii) as discontinuities in the instantaneous frequencies, and (iii) as high gradients of the slope in the instantaneous phases. In a second stage, instantaneous frequencies associated with a time interval experiencing a post-yield stiffness have been used to quantify the change. Two alternative statistical methods have been tested for exploring the solution space: cross-entropy and Bayesian statistics. Bayesian statistics have shown to be more robust and faster than cross-entropy. The level of post-yield stiffness has been successfully quantified for different stiffness losses and speeds of the moving load.

Although preliminary results in this paper have been promising, it is acknowledged that in a field test, the values of parameters of the theoretical model assumed to be known may be inaccurate or simply unavailable. Corrupted measurements and poor selection of parameters for the theoretical model due to wrong assumptions will unavoidably lead to a loss of accuracy in the estimation of the variable/s targeted by an HHT-statistical optimization process. Therefore, further fieldwork and theoretical simulations are needed to investigate how uncertainties associated with damping, noise, a full vehicle-bridge interaction system and/or more than one source of

non-linearity can affect the performance of the proposed method for identifying and quantifying transitory stiffness changes in a structure.

6 ACKNOWLEDGEMENTS

The authors would like to express their gratitude for the financial support received from the Output-Based Research Support Scheme (OBRSS) and the PhD in Sustainable Development Programme at University College Dublin, Ireland, towards this investigation. At a personal level, the authors would like to sincerely thank Dr Salam Al-Sabah for his help in verifying the bi-linear model.

7 REFERENCES

- Aied, H., Gonzalez, A. & Cantero, D. 2016. Identification of sudden stiffness changes in the acceleration response of a bridge to moving loads using ensemble empirical mode decomposition. *Mechanical Systems and Signal Processing* 66: 314–338.
- Cheng, F.Y. 2000. *Matrix analysis of structural dynamics: applications and earthquake engineering*. CRC Press.
- Chen, B., Zhao, S.-L. & Li, P.-Y. 2014. Application of Hilbert-Huang Transform in structural health monitoring: a state-of-the-art review. *Mathematical Problems in Engineering* 2014(7): 1–22.
- Clough, R.W. & Penzien, J. 1993. *Dynamics of structures*, 2nd edition. McGraw-Hill, New York.
- Craig, R.R. 1981. *Structural dynamics: an introduction to computer methods vol. 40*, Wiley New York.
- Dowling, J., OBrien, E.J. & González, A. 2012. Adaptation of cross-entropy optimisation to a dynamic Bridge WIM calibration problem. *Engineering Structures* 44: 13–22.
- Earls, C.J. 2013. Bayesian inference of hidden corrosion in steel bridge connections: Non-contact and sparse contact approaches. *Mechanical Systems and Signal Processing* 41: 420–432.
- Farrar, C.R., Worden, K., Todd, M.D., Park, G., Nichols, J., Adams, D.E., Bement, M.T. & Farinholt, K. 2007. *Nonlinear system identification for damage detection*. LA-14353, Los Alamos National Laboratories, Los Alamos, NM.
- Feldman, M. 1994. Non-linear system vibration analysis using Hilbert transform--II. Forced vibration analysis method 'Forcevib'. *Mechanical Systems and Signal Processing* 8: 309–318.
- Frank Pai, P. 2010. Instantaneous frequency of an arbitrary signal. *International Journal of Mechanical Sciences* 52: 1682–1693.
- Gelman, A., Carlin, J.B. Stern, H.S. & Rubin, D.B. 2003. *Bayesian data analysis*, 2nd edition, Taylor & Francis.
- González, A., Covián, E., Casero, M. & Cooper, J. 2013. Experimental testing of a cross-entropy algorithm to detect damage. *Key Engineering Materials* 569: 1170–1177.
- González, A. & Aied, H. 2015. Characterization of non-linear bearings using the Hilbert-Huang transform. *Advances in Mechanical Engineering* 7(4): 1–13.
- Hester, D. & González, A. 2012. A wavelet-based damage detection algorithm based on bridge acceleration response to a vehicle. *Mechanical Systems and Signal Processing* 28: 145–166.
- Huang, N.E., Shen, Z., Long, S.R., Wu, M.C., Shih, H.H., Zheng, Q., Yen, N.C., Tung, C.C. & Liu, H.H. 1998. The empirical mode decomposition and the Hilbert spectrum for nonlinear and non-stationary time series analysis. *Proceedings of the Royal Society A: Mathematical, Physical and Engineering Sciences* 454: 903–995.
- Huang, N.E. & Shen, S.S. 2005. *Hilbert-Huang transform and its applications*. Singapore; Hackensack, NJ; London: World Scientific.
- Huang, H. & Pan, J. 2006. Speech pitch determination based on Hilbert-Huang transform. *Signal Processing* 86: 792–803.
- Kalvoda, T. & Hwang, Y.-R. 2010. Analysis of signals for monitoring of nonlinear and non-stationary machining processes. *Sensors and Actuators A: Physical* 161(1-2): 39–45.
- Kerschen, G., Vakakis, A.F., Lee, Y., McFarland, D. & Bergman, L. 2008. Toward a fundamental understanding of the Hilbert-Huang transform in nonlinear structural dynamics. *Journal of Vibration and Control* 14: 77–105.
- Kijewski-Correa, T. & Kareem, A. 2006. Efficacy of Hilbert and wavelet transforms for time-frequency analysis. *ASCE Journal of Engineering Mechanics* 132: 1037–1049.

- Kunwar, A., Jha, R., Whelan, M. & Janoyan, K. 2013. Damage detection in an experimental bridge model using Hilbert-Huang transform of transient vibrations. *Structural Control and Health Monitoring* 20: 1–15.
- Lee, J. 2009. Identification of multiple cracks in a beam using natural frequencies. *Journal of Sound and Vibration* 320: 482–490.
- Li, J., Law, S.S. & Hao, H.J. 2013. Improved damage identification in bridge structures subject to moving loads: Numerical and experimental studies. *International Journal of Mechanical Sciences* 74: 99–111.
- Marwala, T. 2010. *Finite-element-model updating using computational intelligence techniques: applications to structural dynamics*. Springer.
- Meredith, J., González, A. & Hester, D. 2012. Empirical mode decomposition of the acceleration response of a prismatic beam subject to a moving load to identify multiple damage locations. *Shock and Vibration Digest* 19: 845–856.
- Mthembu, L., Marwala, T., Friswell, M.I. & Adhikari, S. 2011. Model selection in finite element model updating using the Bayesian evidence statistic. *Mechanical Systems and Signal Processing* 25: 2399–2412.
- Muto, M. & Beck, J.L. 2008. Bayesian updating and model class selection for hysteretic structural models using stochastic simulation. *Journal of Vibration and Control* 14: 7–34.
- Nagarajaiah, S. & Basu, B. 2009. Output only modal identification and structural damage detection using time-frequency & wavelet techniques. *Earthquake Engineering and Engineering Vibration* 8(4): 583–605.
- Neal, R.M. 1993. *Probabilistic inference using Markov chain Monte Carlo methods*. Technical Report CRG-TR-93-1, Department of Computer Science, University of Toronto.
- Nichols, J.M., Link, W.A., Murphy, K.D. & Olson, C.C. 2010. A Bayesian approach to identifying structural nonlinearity using free-decay response: Application to damage detection in composites. *Journal of Sound and Vibration* 329: 2995–3007.
- Nichols, J.M., Moore, E.Z. & Murphy, K.D. 2011. Bayesian identification of a cracked plate using a population-based Markov Chain Monte Carlo method. *Computers & Structures* 89: 1323–1332.
- Nickel, R.E. 1971. On the stability of approximation operators in problems of structural dynamics. *International Journal of Solids and Structures* 7: 301–319.
- Pålsson, R. & Mirza, M.S. 2002. Mechanical response of corroded steel reinforcement of abandoned concrete bridge. *ACI Structural Journal* 99(2): 157–162.
- Pinkaew, T. & Asnachinda, P. 2007. Experimental study on the identification of dynamic axle loads of moving vehicles from the bending moments of bridges. *Engineering Structures* 29: 2282–2293.
- Pugasap, K. 2006. *Hysteresis based model prediction of integral abutment bridge behavior*. PhD thesis, College of Engineering, Pennsylvania State University, Pennsylvania.
- Quek, S.T., Tua, P.S. & Wang, Q. 2003. Detecting anomalies in beams and plate based on the Hilbert-Huang transform of real signals. *Smart Materials and Structures* 12(3): 447–460.
- Roveri, N. & Carcaterra, A. 2012. Damage detection in structures under traveling loads by Hilbert-Huang transform. *Mechanical Systems and Signal Processing* 28: 128–144.
- Song, J. & Der Kiureghian, A. 2006. Generalized Bouc–Wen model for highly asymmetric hysteresis. *ASCE Journal of Engineering Mechanics* 132: 610–618.
- Stewart, M.G. & Al-Harthy, A. 2008. Pitting corrosion and structural reliability of corroding RC structures: Experimental data and probabilistic analysis. *Reliability Engineering & System Safety* 93: 373–382.
- Stewart, M.G. 2009. Mechanical behaviour of pitting corrosion of flexural and shear reinforcement and its effect on structural reliability of corroding RC beams. *Structural Safety* 31: 19–30.
- Wang, C., Ren, W.-X., Wang, Z.-C. & Zhu, H.-P. 2013. Instantaneous frequency identification of time-varying structures by continuous wavelet transform. *Engineering Structures* 52: 17–25.
- Wu, M. & Smyth, A.W. 2007. Application of the unscented Kalman filter for real-time nonlinear structural system identification. *Structural Control and Health Monitoring* 14: 971–990.
- Wu, Z. & Huang, N.E. 2009. Ensemble empirical mode decomposition: a noise-assisted data analysis method. *Advances in Adaptive Data Analysis* 1: 1–41.
- Yang, J.N., Lei, Y., Lin, S. & Huang, N. 2003. Hilbert-Huang based approach for structural damage detection. *ASCE Journal of Engineering Mechanics* 130: 85–95.
- Zeynalian, M., Ronagh, H.R. & Dux, P. 2012. Analytical description of pinching, degrading, and sliding in a bilinear hysteretic system. *ASCE Journal of Engineering Mechanics* 138: 1381–1387.